CRYSTAL GROWTH & DESIGN

pubs.acs.org/crystal Article

Chiral Resolution of *RS*-Oxiracetam upon Cocrystallization with Pharmaceutically Acceptable Inorganic Salts

Oleksii Shemchuk, Lixing Song, Nikolay Tumanov, Johan Wouters, Dario Braga, Fabrizia Grepioni,* and Tom Leyssens*

Cite This: *Cryst. Growth Des.* 2020, 20, 2602−2607 Read Online

ACCESS | Metrics & More | Article Recommendations | Supporting Information

ABSTRACT: Ionic cocrystals (ICCs) of racemic *RS*-oxiracetam and of its active *S*-enantiomer of pharmaceutical interest with the pharmaceutically acceptable salts calcium and magnesium chloride were synthesized and structurally characterized. The cocrystallization of *RS*-oxiracetam with $MgCl_2$ resulted in chiral resolution with formation of an *S*-OXI·$MgCl_2$·$5H_2O$/*R*-OXI·$MgCl_2$·$5H_2O$ conglomerate. Ternary phase diagrams of *RS*-oxiracetam/inorganic salt/solvent were constructed to determine the overall compositions for which the ICCs are the only stable phases in suspension. In addition, single crystals of *S*-oxiracetam were grown, and its structure was determined.

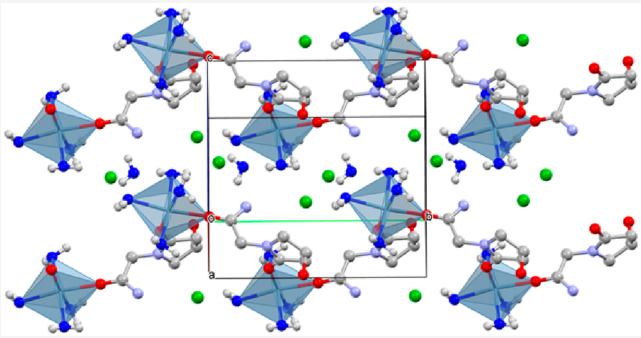

INTRODUCTION

Cocrystals in general, and ionic cocrystals (ICCs) in particular, have become attractive research topics in the pharmaceutical industry, since they can provide an alternative route to new pharmaceutical formulations compared to conventional salts.[1−7] A virtually infinite choice of molecular and/or ionic building blocks makes the number of possible combinations between active pharmaceutical ingredients (APIs) and ancillary coformers or other APIs limitless. ICCs belong to a class of multicomponent crystalline solids composed of neutral organic molecules and salts in a defined stoichiometric ratio.[8−15] Pharmaceutical ICCs are of particular interest, since they can modulate the physicochemical and biological properties of the APIs (e.g., bioavailability, solubility, intrinsic dissolution rate, morphology, stability toward humidity, and thermostability) in an impressive manner.[16−20] The formulation of drugs as cocrystals can be especially important with APIs that lack ionizable moieties, which therefore cannot be formulated and used as conventional salts. Enantiopure and racemic oxiracetam (see Scheme 1) investigated in this work belong to such APIs.

Oxiracetam (4-hydroxy-2-oxo-l-pyrrolidineacetamide, hydroxypiracetam) is a nootropic drug of the racetam family and is a very mild stimulant.[21] It was also tested for potential use in different forms of dementia, and it was reported to have no side effects. Oxiracetam showed beneficial effects on logical performance, attention, concentration, and memory.[21−23] Some studies showed that oxiracetam was more effective than the prototype nootropic piracetam.[24]

Oxiracetam was first synthesized by Smith Kline Beecham Company in 1974 as a racemate.[25] However, as typical for the majority of chiral drugs, only one enantiomer (*S*-oxiracetam) exerts the desired biological properties.[21] Therefore, marketing of oxiracetam as a pure enantiomer, in principle, could be interesting. Furthermore, the general trend in the pharmaceutical industry is to evolve toward development of chiral medicines in enantiomerically enriched and ideally pure form.[26] However, *S*-oxiracetam was found by Wang et al. to

Scheme 1. Chemical Structures[a]

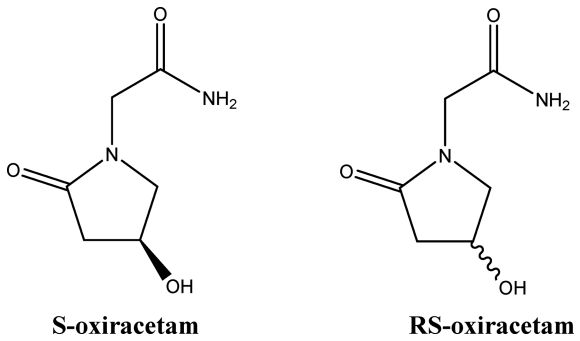

[a]Chemical structures of enantiopure (left) and racemic (right) oxiracetam.

Received: December 28, 2019
Revised: February 20, 2020
Published: February 20, 2020

be heavily hygroscopic with deliquescence occurring after a 3 d hold at 87% relative humidity (RH) and 25 °C.[25] They successfully tried to enhance the hygroscopic stability of *S*-oxiracetam upon its cocrystallization with gallic and 3,4-dihydroxybenzoic acids.[25] Even though the crystal structures of these cocrystals were given in the manuscript,[25] the structure of enantiopure oxiracetam has not been reported so far. In the Cambridge Structural Database (CSD)[27] only the structure of racemic oxiracetam is available.[28]

The impact of cocrystallization on the chirality of pharmaceutical compounds has been thoroughly investigated by our research groups. The formation of molecular[29] and ionic[30,31] cocrystals was found to be a suitable technique to achieve chiral resolution of racemic mixtures. Cocrystallization of the amino acids D,L-histidine and D,L-proline with lithium halides showed the possibility to perform chiral resolution,[30,31] as Li^+ linked selectively with amino acids of only one chirality, with formation of conglomerates or of racemic crystals but constituted of homochiral chains, while the use of calcium[32] halides led to cocrystallization of racemic ICCs. Chiral resolution was obtained also via coordination of levetiracetam (*S*-etiracetam) and *RS*-etiracetam to $ZnCl_2$:[33] in this work chiral resolution was attempted by varying the stoichiometric ratio of the coformer, thus enabling a reversible switch between a thermodynamically stable racemic compound and conglomerate. On the basis of the results concerning the Li^+ and Zn^{2+} cations, it was initially assumed that the tetrahedral geometry around the cation was a prerequisite for the segregation, in individual chains or crystals, of molecules of the same handedness. However, in our latest paper[34] we showed that the cocrystallization of etiracetam with both $CaCl_2$ and $MgCl_2$ resulted in the formation of homochiral layers of octahedrally coordinated calcium and magnesium cations.

In this paper we explore the effect of cocrystallizing both enantiopure and racemic oxiracetam with $CaCl_2$ and $MgCl_2$, both pharmaceutically acceptable inorganic salts. Ternary phase diagrams (TPDs) for the system *RS*-oxiracetam/inorganic salt/solvent were constructed, to determine the overall compositions for which the ICCs were the only stable phases in suspension. We furthermore identified conditions for the system *RS*-oxiracetam/$MgCl_2$/ethanol 70%, which can be used to develop a resolution by *entrainment* (preferential crystallization).[35,36] Crystalline *S*-oxiracetam was also structurally characterized.

■ EXPERIMENTAL PART

Materials and Instrumentation. *RS*-Oxiracetam and *S*-oxiracetam were purchased from Xiamen Top Health Biochem Tech. Co., Ltd. All the other reagents were purchased from Sigma and used without further purification.

Single crystals of *S*-oxiracetam of suitable quality for X-ray analysis were grown through evaporation of an acetonitrile solution at 60 °C. Ten milligrams of *S*-oxiracetam were dissolved in 15 mL of acetonitrile upon heating. The solution was left to evaporate at 60 °C.

Solution Synthesis. *S*-OXI·$CaCl_2$·$5H_2O$, *S*-OXI·$MgCl_2$·$5H_2O$, and OXI_2·$CaCl_2$ were obtained by slow evaporation from aqueous solution (3 mL) of stoichiometric quantities (117.5−41.3 mg for OXI_2·$CaCl_2$ and 62.4−37.6 mg for *R*-OXI·$MgCl_2$·$5H_2O$/*S*-OXI·$MgCl_2$·$5H_2O$) of the reagents (2:1 for OXI_2·$CaCl_2$ and 1:1 for the rest) at room temperature. The evaporation process over a period of 10−30 d resulted in the formation of an oil-like product.

Slurry Synthesis. OXI_2·$CaCl_2$ was also obtained by slurrying a stoichiometric amount of oxiracetam and $CaCl_2$ (235 mg −82.5 mg) for 2 d at 25 °C in 5 mL of absolute ethanol, whereas the conglomerate mixture *R*-OXI·$MgCl_2$·$5H_2O$/*S*-OXI·$MgCl_2$·$5H_2O$ was obtained slurrying a stoichiometric mixture in 70% ethanol (see Section S4, Supporting Information).

Mechanochemical Synthesis. OXI_2·$CaCl_2$ and *R*-OXI·$MgCl_2$·$5H_2O$/*S*-OXI·$MgCl_2$·$5H_2O$ were obtained mechanochemically by ball-milling stoichiometric ratios of the starting materials (117.5−41.3 mg for OXI_2·$CaCl_2$ and 62.4−37.6 mg for *R*-OXI·$MgCl_2$·$5H_2O$/*S*-OXI·$MgCl_2$·$5H_2O$) in stainless steel jars for 15 min in a Retsch MM200 ball miller operated at a frequency of 20 Hz, using stainless steel jars (5 mL) and two 3 mm balls, with the addition of a drop of water.

Thermogravimetric Analysis. Thermogravimetric (TG) analyses were performed with a PerkinElmer TGA7 in the temperature range of 40−500 °C under N_2 gas flow at a heating rate of 5.00 °C min^{-1}.

Differential Scanning Calorimetry. Differential scanning calorimetry (DSC) thermograms were recorded using a PerkinElmer Diamond. The samples (1−3 mg range), obtained via kneading, were placed in open Al pans. All measurements were conducted at a heating rate of 5 or 10 °C min^{-1}.

X-ray Diffraction from Powder. For phase identification purposes X-ray powder diffraction (XRPD) patterns were collected on a PANalytical X′Pert Pro Automated diffractometer equipped with an X′celerator detector in Bragg−Brentano geometry, using Cu Kα radiation (λ = 1.5418 Å) without monochromator in 3−50° 2θ range (step size 0.033°; time/step: 20 s; Soller slit 0,04 rad, antiscatter slit: 1/2, divergence slit: 1/4 ; 40 mA × 40 kV).

Single-Crystal X-ray Diffraction. *S-Oxiracetam.* Single-crystal X-ray diffraction data were collected using an Oxford Diffraction Gemini R Ultra diffractometer (Cu Kα, multilayer mirror, Ruby CCD area detector) at 295(2) K. Data collection, unit cells determination, and data reduction were performed using CrysAlis PRO software package[37] using Olex2[38] interface. The structure was solved with the SHELXT 2015[39] structure solution program by Intrinsic Phasing methods and refined by full-matrix least-squares on $|F|^2$ using SHELXL-2018/3.[40] Non-hydrogen atoms were refined anisotropically. All hydrogen atoms were located from a Fourier map. Hydrogen atoms not involved in hydrogen bonding were placed on calculated positions in riding mode with temperature factors fixed at 1.2 times U_{eq} of the parent carbon atoms. H_{OH} and H_{NH} atoms were refined riding on their respective nitrogen or oxygen atoms (X−H distances were refined). Absolute configuration of the sample was established by anomalous-dispersion effects in diffraction measurements on the crystal. The Flack *x* parameter was determined using 1125 quotients $[(I_+) - (I_-)]/[(I_+) + (I_-)]$[41] and equal to 0.07(8).

$CaCl_2$ and $MgCl_2$ ICCs. Single-crystal data were collected at room temperature with an Oxford Diffraction X′Calibur equipped with a graphite monochromator and a CCD detector. Mo Kα radiation (λ = 0.710 73 Å) was used. Unit cell parameters for both complexes discussed herein are reported in Table SI-1. The structure was solved by the Intrinsic Phasing methods and refined by least-squares methods against F^2 using SHELXT-2014[42] and SHELXL-2018[40] with Olex2 interface.[38] Non-hydrogen atoms were refined anisotropically. H_{CH} atoms were added in calculated positions; H_{OH} and H_{NH} atoms were either located from a Fourier map or added in calculated positions and refined riding on their respective carbon, nitrogen, or oxygen atoms. The software Mercury 4.0[43] and VESTA[44] were used for graphical representations and for powder patterns simulation on the basis of single-crystal data.

Ternary Phase Diagram. TPDs were constructed by slurrying oxiracetam with $CaCl_2$ and $MgCl_2$ in absolute and 70% ethanol, respectively, varying the molar ratio of the starting materials from 0 to 1. Experiments were performed in a number of 2 mL sealed vials, and the suspensions were stirred at constant temperature (25 °C) for at least 48 h. Seeding with all possible solid-state forms was performed to make sure that the system reached thermodynamic equilibrium. Afterward the samples were filtered by sand core funnel, and the obtained solids were characterized by XRPD. To determine the equilibrium compositions required for the determination of the solubility lines, all the experiments described above were repeated up to the filtration step. After slurrying for 48 h, small portions of solvent were added to the stirring mixtures every 30 min, until complete

https://dx.doi.org/10.1021/acs.cgd.9b01725
Cryst. Growth Des. 2020, 20, 2602−2607

dissolution of the suspended solid was observed. This allowed the construction of the solubility line in the ternary phase diagram. TPDs were drawn with the software ProSim Ternary Diagram. For detailed information see the Supporting Information.

RESULTS AND DISCUSSION

S-Oxiracetam. Single crystals of *S*-oxiracetam suitable for X-ray structure determination were grown from hot acetonitrile, due to the high hygroscopicity of the compound. *S*-Oxiracetam (Figure 1) crystallizes in the monoclinic $P2_1$ space group with two molecules in the asymmetric unit cell (for detailed structural information on this and the other solids discussed in this paper see Table SI-1).

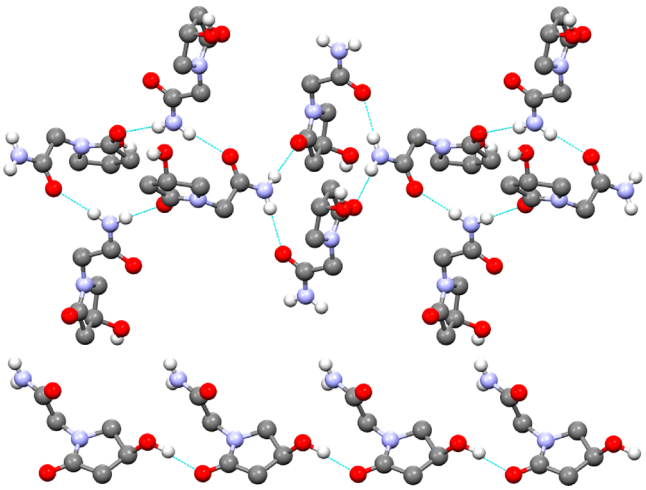

Figure 1. Hydrogen-bonding patterns of the type $-NH\cdots O_{CO}$ (top) and $-OH\cdots O_{CO}$ (bottom) in crystalline *S*-oxiracetam. H_{CH} omitted for clarity.

Cocrystallization of *S*-oxiracetam with $CaCl_2$ and $MgCl_2$ (see Supporting Information) resulted in the formation of the isomorphous solids *S*-OXI·$CaCl_2$·$5H_2O$ (Figure 2) and *S*-OXI·$MgCl_2$·$5H_2O$ (Figure SI-2).

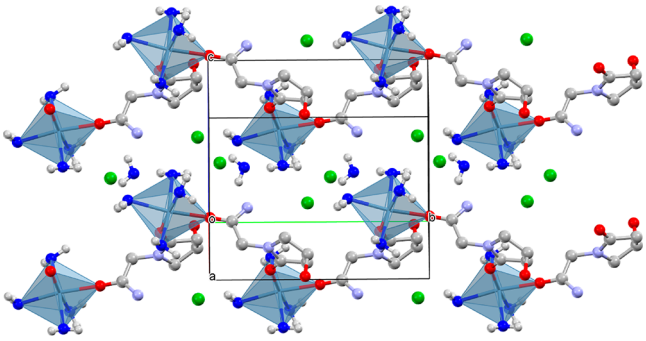

Figure 2. Crystal packing of *S*-OXI·$CaCl_2$·$5H_2O$, showing the 1D chains extending along the crystallographic *b*-axis. Water oxygens in blue; H atoms omitted for clarity.

As it can be seen in Figure 2, two *S*-oxiracetam molecules and four water molecules are coordinated to the Ca^{2+} cation via the oxygen atoms in an octahedral fashion. The fifth water molecule is hydrogen-bonded to the chloride anions and to the water molecules of the first coordination sphere. Each *S*-oxiracetam molecule interacts in turn with a second calcium cation, thus forming infinite chains extending along the crystallographic *b*-axis.

RS-Oxiracetam. *RS*-Oxiracetam (oxiracetam hereafter) was also cocrystallized with magnesium and calcium chlorides, and, differently from what observed with the enantiopure *S*-oxiracetam, the use of the two inorganic salts yielded two different products. Oxiracetam formed with $CaCl_2$ the racemic OXI_2·$CaCl_2$ (Figure 3), which, quite surprisingly, is anhydrous, in contrast to the majority of ICCs obtained with racetams and calcium chloride.[32,45] Crystalline OXI_2·$CaCl_2$ is characterized, as in the case of the enantiopure *S*-OXI·$CaCl_2$·$5H_2O$, by an octahedral coordination around the calcium cation, but in the racemate four oxiracetam molecules provide all the necessary oxygen atoms to the central calcium cation. As the Ca^{2+} ions are located on inversion centers, the four oxiracetam molecules are divided in two pairs of opposite chirality (two *R*- and two *S*-oxiracetam molecules). Each oxiracetam molecule, in turn, is coordinated to two calcium cations. Once again the coordination to the metal center results in the formation of infinite one-dimensional (1D) chains, which extend along the crystallographic *b*-axis direction, as shown in Figure 3.

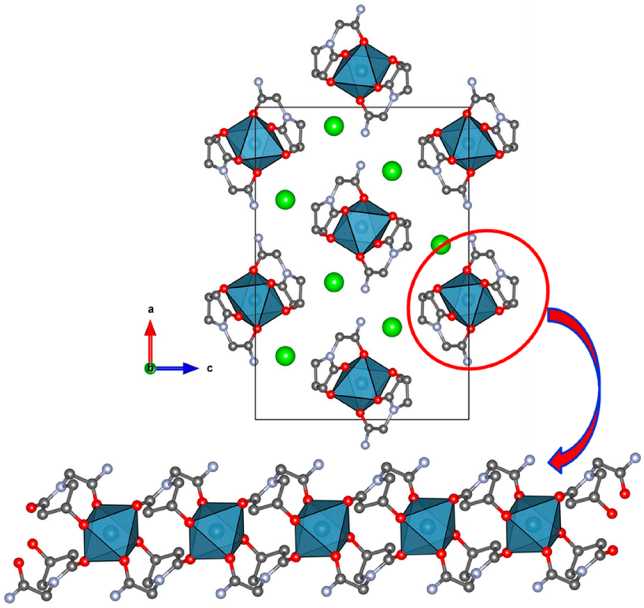

Figure 3. Packing arrangement of the 1D chains and the chloride ions in crystalline OXI_2·$CaCl_2$ (top) and a single chain showing the involvement of all oxygen atoms in the coordination to the calcium cations (bottom). H atoms omitted for clarity.

Cocrystallization of oxiracetam with $MgCl_2$ resulted in spontaneous chiral resolution, with formation of a stable *S*-OXI·$MgCl_2$·$5H_2O$/*R*-OXI·$MgCl_2$·$5H_2O$ conglomerate. Chiral resolution was observed in all cocrystallization methods applied, whether ball milling with a drop of water, slow evaporation from undersaturated aqueous, ethanol and methanol solutions, or by slurry. The cocrystal is always found as a pentahydrate phase. TPDs for oxiracetam/$MgCl_2$/ethanol were then determined, which helped to identify the thermodynamically stable equilibrium for different overall compositions at a given temperature and pressure (see Figure 4 and Figure SI-16). The choice of the solvent is important for the overall aspect of this diagram, as oxiracetam is almost insoluble in absolute ethanol and extremely soluble in water. A series of experiments was performed to identify the water–

https://dx.doi.org/10.1021/acs.cgd.9b01725
Cryst. Growth Des. 2020, 20, 2602−2607

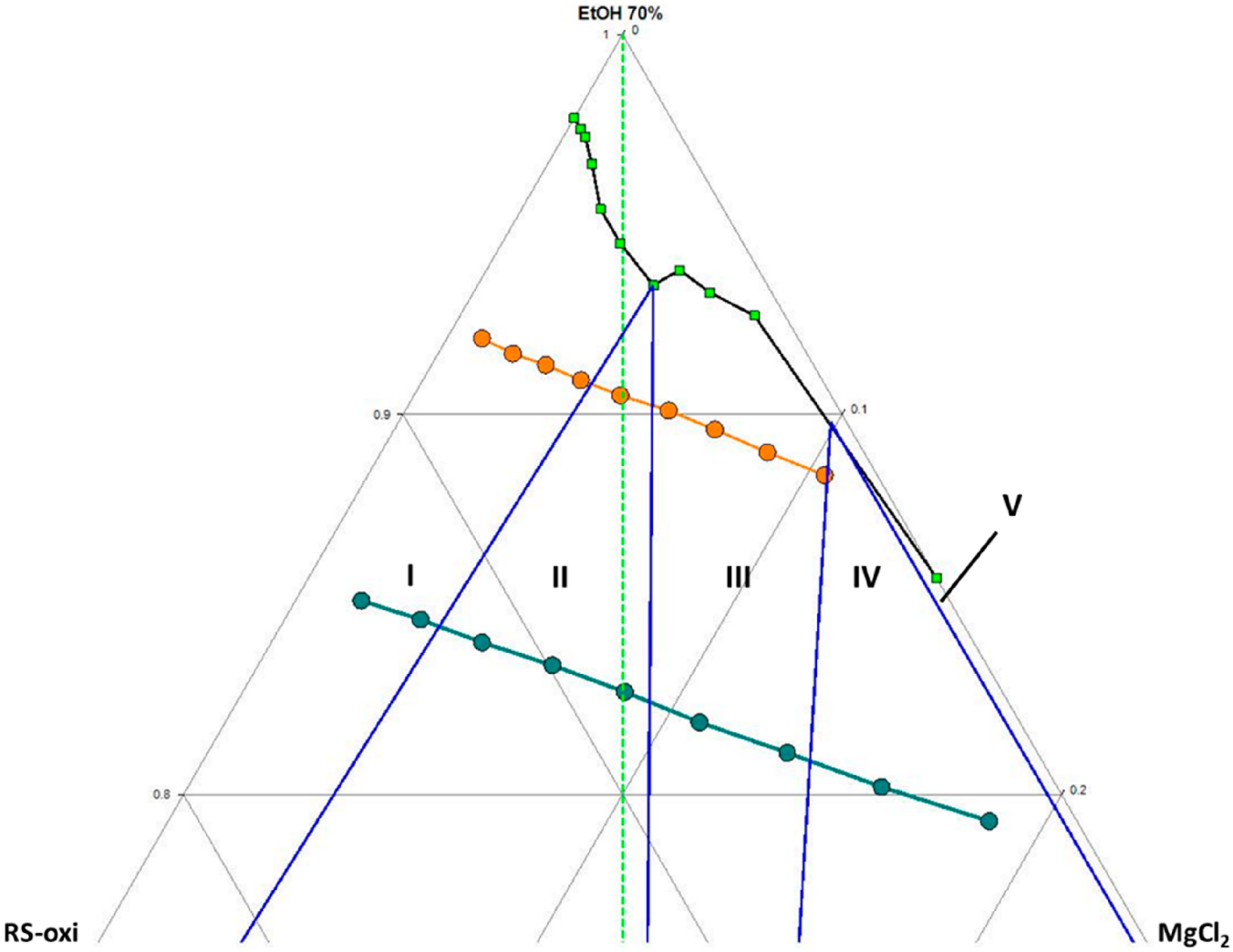

Figure 4. Enlarged portion of the TPD for *RS*-OXI/$MgCl_2$/70% EtOH at 298 K (mol %) [For the full version see Figure SI-17].

ethanol mixture that led to the largest stability zone for the conglomerate suspension. This occurred for a 70% ethanol composition of the solvent. Detailed information on the construction of the given TPD is given in the Supporting Information.

The experimental ternary phase diagram (see Figure 4 and Figure SI-17) shows two biphasic regions (**I** = *RS*-OXI + L and **V** = $MgCl_2$ + L), one triphasic region (**III** = *S*-OXI·$MgCl_2$·$5H_2O$ + *R*-OXI·$MgCl_2$·$5H_2O$ + L), and two quadriphasic regions (**II** = *RS*-OXI + *S*-OXI·$MgCl_2$·$5H_2O$ + *R*-OXI·$MgCl_2$·$5H_2O$ + L and **IV** = $MgCl_2$ + *S*-OXI·$MgCl_2$·$5H_2O$ + *R*-OXI·$MgCl_2$·$5H_2O$ + L); L is the liquid phase. It is worth stressing that these phase diagrams can be used to develop a full resolution by *entrainment* (preferential crystallization),[35,36] by targeting the triphasic region **III**, where the conglomerate is the only thermodynamically stable phase in suspension. If the pure drug is the target, of course, at the end of the process the cocrystal would need to be "dismantled". This could be achieved via suspension of the cocrystal in a solvent in which the organic compound is highly soluble, while the inorganic salt is not: the cocrystal will likely behave incongruently, with the salt crystallizing out and *S*-oxiracetam remaining in solution. A similar methodology has recently been applied for the separation of active pharmaceutical ingredients as enantiopure (*S*)-ibuprofen[46,47] and leviracetam.[47]

Considering *S*-OXI·$MgCl_2$·$5H_2O$ and *S*-OXI·$CaCl_2$·$5H_2O$ to be isostructural, a number of attempts were made to try and force conglomerate formation for the *RS*-oxiracetam $CaCl_2$ system also. Attempts were made by (i) introducing seeds of *S*-OXI·$MgCl_2$·$5H_2O$/*R*-OXI·$MgCl_2$·$5H_2O$ (10%) into the oil formed upon evaporation of the undersaturated oxiracetam: $CaCl_2$ solution, (ii) simultaneous cocrystallizing $CaCl_2$ and $MgCl_2$ (0.05 + 0.05 mmol) with oxiracetam (0.1 mmol) through slow solvent evaporation, and (iii) performing a number of ball-milling experiments varying the stoichiometric ratio of $CaCl_2$/$MgCl_2$. Unfortunately, none of these experiments yielded formation of a $CaCl_2$ conglomerate. The ball milling always resulted in the formation of a physical mixture of *S*-OXI·$MgCl_2$·$5H_2O$/*R*-OXI·$MgCl_2$·$5H_2O$ and OXI_2·$CaCl_2$, whereas crystallization from solution always led to the formation of *S*-OXI·$MgCl_2$·$5H_2O$/*R*-OXI·$MgCl_2$·$5H_2O$ crystals with $CaCl_2$ and the unreacted oxiracetam remaining in the liquid/oil phase.

■ CONCLUSIONS

The formation of both molecular and ionic cocrystals represents a promising technique to perform chiral resolution of racemic mixtures. In this work ICCs of both racemic and enantiopure oxiracetam with the pharmaceutically acceptable

https://dx.doi.org/10.1021/acs.cgd.9b01725
Cryst. Growth Des. 2020, 20, 2602−2607

salts $CaCl_2$ and $MgCl_2$ have been obtained and structurally characterized. The cocrystallization of *RS*-oxiracetam with $MgCl_2$ led to chiral resolution with formation of an *S*-OXI·$MgCl_2$·$5H_2O$/*R*-OXI·$MgCl_2$·$5H_2O$ conglomerate. In these solids the Mg^{2+} cations are octahedrally coordinated, and this is the first observation of chiral resolution achieved by cocrystallization with a metal in this type of coordination. Considering these results and the fact that the cocrystallization of etiracetam with $CaCl_2$ and $MgCl_2$ also resulted in formation of homochiral layers around calcium and magnesium cations, it might be concluded that the phenomenon of homochiral preference of metal cations goes beyond the tetrahedral geometry around the metal cation and is driven by even subtler conditions. This study also showed that ternary phase diagrams can be easily constructed allowing identification of those zones where ICCs are the only stable phases in suspension and where entrainment can be performed.

■ ASSOCIATED CONTENT

Supporting Information

The Supporting Information is available free of charge at https://pubs.acs.org/doi/10.1021/acs.cgd.9b01725.

TGA, DSC, XRPD patterns, TPDs (PDF)

Accession Codes

CCDC 1972456−1972459 contain the supplementary crystallographic data for this paper. These data can be obtained free of charge via www.ccdc.cam.ac.uk/data_request/cif, or by emailing data_request@ccdc.cam.ac.uk, or by contacting The Cambridge Crystallographic Data Centre, 12 Union Road, Cambridge CB2 1EZ, U.K.; fax: + 44 1223 336033.

■ AUTHOR INFORMATION

Corresponding Authors

Fabrizia Grepioni − *Molecular Crystal Engineering Laboratory, Dipartimento di Chimica "G. Ciamician", Università di Bologna, 40126 Bologna, Italy;* orcid.org/0000-0003-3895-0979; Email: fabrizia.grepioni@unibo.it

Tom Leyssens − *Institute of Condensed Matter and Nanosciences, Université catholique de Louvain, B-1348 Louvain-La-Neuve, Belgium*; Email: tom.leyssens@uclouvain.be

Authors

Oleksii Shemchuk − *Molecular Crystal Engineering Laboratory, Dipartimento di Chimica "G. Ciamician", Università di Bologna, 40126 Bologna, Italy;* orcid.org/0000-0003-3003-3922

Lixing Song − *Institute of Condensed Matter and Nanosciences, Université catholique de Louvain, B-1348 Louvain-La-Neuve, Belgium;* orcid.org/0000-0003-4874-3551

Nikolay Tumanov − *Unité de Chimie Physique Théorique et Structurale, Chemistry Department, Namur Institute of Structured Matter, University of Namur, B-5000 Namur, Belgium;* orcid.org/0000-0001-6898-9036

Johan Wouters − *Unité de Chimie Physique Théorique et Structurale, Chemistry Department, Namur Institute of Structured Matter, University of Namur, B-5000 Namur, Belgium*

Dario Braga − *Molecular Crystal Engineering Laboratory, Dipartimento di Chimica "G. Ciamician", Università di Bologna, 40126 Bologna, Italy;* orcid.org/0000-0003-4162-4779

Complete contact information is available at: https://pubs.acs.org/10.1021/acs.cgd.9b01725

Notes

The authors declare no competing financial interest.

■ ACKNOWLEDGMENTS

This material is based on the work of L.S., supported by the China Scholarship Council and FNRS (PDR T.0149.19). The Universities of Bologna (O.S., D.B., and F.G.−RFO scheme) and Namur (N.T. and J.W.), and the Université Catholique de Louvain (T.L.), are also acknowledged.

■ REFERENCES

(1) Almarsson, O.; Zaworotko, M. J. Crystal engineering of the composition of pharmaceutical phases. Do pharmaceutical co-crystals represent a new path to improved medicines? *Chem. Commun.* **2004**, 1889−1896.

(2) Vishweshwar, P.; McMahon, J. A.; Bis, J. A.; Zaworotko, M. J. Pharmaceutical co-crystals. *J. Pharm. Sci.* **2006**, *95*, 499−516.

(3) Schultheiss, N.; Newman, A. Pharmaceutical Cocrystals and Their Physicochemical Properties. *Cryst. Growth Des.* **2009**, *9*, 2950−2967.

(4) Yadav, A. V.; Shete, A. S.; Dabke, A. P.; Kulkarni, P. V.; Sakhare, S. S. Co-crystals: a novel approach to modify physicochemical properties of active pharmaceutical ingredients. *Indian J. Pharm. Sci.* **2009**, *71*, 359−70.

(5) Good, D. J.; Rodriguez-Hornedo, N. Solubility Advantage of Pharmaceutical Cocrystals. *Cryst. Growth Des.* **2009**, *9*, 2252−2264.

(6) Wouters, J.; Quéré, L. *Pharmaceutical salts and co-crystals;* Royal Society of Chemistry, 2011.

(7) Jones, W.; Motherwell, W. D. S.; Trask, A. V. Pharmaceutical Cocrystals: An Emerging Approach to Physical Property Enhancement. *MRS Bull.* **2006**, *31*, 875−879.

(8) Braga, D.; Grepioni, F.; Maini, L.; Prosperi, S.; Gobetto, R.; Chierotti, M. R. From unexpected reactions to a new family of ionic co-crystals: the case of barbituric acid with alkali bromides and caesium iodide. *Chem. Commun.* **2010**, *46*, 7715−7.

(9) Smith, A. J.; Kim, S.-H.; Duggirala, N. K.; Jin, J.; Wojtas, L.; Ehrhart, J.; Giunta, B.; Tan, J.; Zaworotko, M. J.; Shytle, R. D. Improving lithium therapeutics by crystal engineering of novel ionic cocrystals. *Mol. Pharmaceutics* **2013**, *10*, 4728−4738.

(10) Kelley, S. P.; Narita, A.; Holbrey, J. D.; Green, K. D.; Reichert, W. M.; Rogers, R. D. Understanding the effects of ionicity in salts, solvates, co-crystals, ionic co-crystals, and ionic liquids, rather than nomenclature, is critical to understanding their behavior. *Cryst. Growth Des.* **2013**, *13*, 965−975.

(11) Delori, A.; Galek, P. T.; Pidcock, E.; Patni, M.; Jones, W. Knowledge-based hydrogen bond prediction and the synthesis of salts and cocrystals of the anti-malarial drug pyrimethamine with various drug and GRAS molecules. *CrystEngComm* **2013**, *15*, 2916−2928.

(12) Butterhof, C.; Bärwinkel, K.; Senker, J.; Breu, J. Polymorphism in co-crystals: a metastable form of the ionic co-crystal 2 HBz· 1 NaBz crystallised by flash evaporation. *CrystEngComm* **2012**, *14*, 6744−6749.

(13) Wang, T.; Stevens, J. S.; Vetter, T.; Whitehead, G. F. S.; Vitorica-Yrezabal, I. J.; Hao, H.; Cruz-Cabeza, A. J. Salts, Cocrystals, and Ionic Cocrystals of a "Simple" Tautomeric Compound. *Cryst. Growth Des.* **2018**, *18*, 6973−6983.

(14) Linberg, K.; Ali, N. Z.; Etter, M.; Michalchuk, A. A. L.; Rademann, K.; Emmerling, F. A Comparative Study of the Ionic Cocrystals NaX (α-d-Glucose)2 (X = Cl, Br, I). *Cryst. Growth Des.* **2019**, *19*, 4293−4299.

(15) Kavanagh, O. N.; Walker, G.; Lusi, M. Graph-Set Analysis Helps To Understand Charge Transfer in a Novel Ionic Cocrystal When the ΔpKa Rule Fails. *Cryst. Growth Des.* **2019**, *19*, 5308−5313.

(16) Duggirala, N. K.; Smith, A. J.; Wojtas, Ł.; Shytle, R. D.; Zaworotko, M. J. Physical stability enhancement and pharmacokinetics of a lithium ionic cocrystal with glucose. *Cryst. Growth Des.* **2014**, *14*, 6135−6142.
(17) Buist, A. R.; Kennedy, A. R. Ionic Cocrystals of Pharmaceutical Compounds: Sodium Complexes of Carbamazepine. *Cryst. Growth Des.* **2014**, *14*, 6508−6513.
(18) Oertling, H. Interactions of alkali-and alkaline earth-halides with carbohydrates in the crystalline state−the overlooked salt and sugar cocrystals. *CrystEngComm* **2016**, *18*, 1676−1692.
(19) Shemchuk, O.; Braga, D.; Maini, L.; Grepioni, F. Anhydrous ionic co-crystals of cyanuric acid with LiCl and NaCl. *CrystEngComm* **2017**, *19*, 1366−1369.
(20) Honer, K.; Kalfaoglu, E.; Pico, C.; McCann, J.; Baltrusaitis, J. Mechanosynthesis of Magnesium and Calcium Salt Urea Ionic Cocrystal Fertilizer Materials for Improved Nitrogen Management. *ACS Sustainable Chem. Eng.* **2017**, *5*, 8546−8550.
(21) Gouliaev, A. H.; Senning, A. Piracetam and other structurally related nootropics. *Brain Res. Rev.* **1994**, *19*, 180−222.
(22) Itil, T. M.; Menon, G. N.; Bozak, M.; Songar, A. The effects of oxiracetam (ISF 2522) in patients with organic brain syndrome (a double-blind controlled study with piracetam). *Drug Dev. Res.* **1982**, *2*, 447−461.
(23) Dager, S. R.; Loebel, J. P.; Claypool, K.; Case, M.; Budech, C. B.; Dunner, D. L. Oxiracetam in the treatment of primary dementia of the Alzheimer's type: A small case series. *Int. J. Geriatr. Psychiatry* **1992**, *7*, 905−912.
(24) Gallai, V.; Mazzotta, G.; Del Gatto, F.; Montesi, S.; Mazzetti, A.; Dominici, P.; Della Monica, A. A clinical and neurophysiological trial on nootropic drugs in patients with mental decline. *Acta neurologica* **1991**, *13*, 1−12.
(25) Wang, Z. Z.; Chen, J. M.; Lu, T. B. Enhancing the Hygroscopic Stability of S-Oxiracetam via Pharmaceutical Cocrystals. *Cryst. Growth Des.* **2012**, *12*, 4562−4566.
(26) Nunez, M. C.; Garcia-Rubino, M. E.; Conejo-Garcia, A.; Cruz-Lopez, O.; Kimatrai, M.; Gallo, M. A.; Espinosa, A.; Campos, J. M. Homochiral drugs: a demanding tendency of the pharmaceutical industry. *Curr. Med. Chem.* **2009**, *16*, 2064−2074.
(27) Groom, C. R.; Bruno, I. J.; Lightfoot, M. P.; Ward, S. C. The Cambridge Structural Database. *Acta Crystallogr., Sect. B: Struct. Sci., Cryst. Eng. Mater.* **2016**, *72*, 171−179.
(28) Bandoli, G.; Grassi, A.; Nicolini, M.; Pappalardo, G. C. Solid-State Structure and Conformation of the Nootropic Agent 4-Hydroxy-2-Oxo-1-Pyrrolidineacetamide - X-Ray and Theoretical Self-Consistant Field Molecular-Orbital (Scf-Mo) Studies. *Chem. Pharm. Bull.* **1985**, *33*, 4395−4401.
(29) Springuel, G.; Leyssens, T. Innovative Chiral Resolution Using Enantiospecific Co-Crystallization in Solution. *Cryst. Growth Des.* **2012**, *12*, 3374−3378.
(30) Braga, D.; Degli Esposti, L.; Rubini, K.; Shemchuk, O.; Grepioni, F. Ionic Cocrystals of Racemic and Enantiopure Histidine: An Intriguing Case of Homochiral Preference. *Cryst. Growth Des.* **2016**, *16*, 7263−7270.
(31) Shemchuk, O.; Tsenkova, B. K.; Braga, D.; Duarte, M. T.; André, V.; Grepioni, F. Ionic Co-crystal Formation as a Path Towards Chiral Resolution in the Solid State. *Chem. - Eur. J.* **2018**, *24*, 12564−12573.
(32) Shemchuk, O.; Degli Esposti, L.; Grepioni, F.; Braga, D. Ionic co-crystals of enantiopure and racemic histidine with calcium halides. *CrystEngComm* **2017**, *19*, 6267−6273.
(33) Shemchuk, O.; Song, L.; Robeyns, K.; Braga, D.; Grepioni, F.; Leyssens, T. Solid-state chiral resolution mediated by stoichiometry: crystallizing etiracetam with $ZnCl_2$. *Chem. Commun.* **2018**, *54*, 10890−10892.
(34) Song, L.; Shemchuk, O.; Robeyns, K.; Braga, D.; Grepioni, F.; Leyssens, T. Ionic Cocrystals of Etiracetam and Levetiracetam: The Importance of Chirality for Ionic Cocrystals. *Cryst. Growth Des.* **2019**, *19*, 2446−2454.
(35) Collet, A.; Brienne, M. J.; Jacques, J. Optical resolution by direct crystallization of enantiomer mixtures. *Chem. Rev.* **1980**, *80*, 215−230.
(36) Levilain, G.; Coquerel, G. Pitfalls and rewards of preferential crystallization. *CrystEngComm* **2010**, *12*, 1983.
(37) *CrysAlisPRO;* Oxford Diffraction /Agilent Technologies UK Ltd: Yarnton, England, 2015.
(38) Dolomanov, O. V.; Bourhis, L. J.; Gildea, R. J.; Howard, J. A. K.; Puschmann, H. OLEX2: a complete structure solution, refinement and analysis program. *J. Appl. Crystallogr.* **2009**, *42*, 339−341.
(39) Sheldrick, G. M. SHELXT - integrated space-group and crystal-structure determination. *Acta Crystallogr., Sect. A: Found. Adv.* **2015**, *71*, 3−8.
(40) Sheldrick, G. M. Crystal structure refinement with SHELXL. *Acta Crystallogr., Sect. C: Struct. Chem.* **2015**, *71*, 3−8.
(41) Parsons, S.; Flack, H. D.; Wagner, T. Use of intensity quotients and differences in absolute structure refinement. *Acta Crystallogr., Sect. B: Struct. Sci., Cryst. Eng. Mater.* **2013**, *69*, 249−59.
(42) Sheldrick, G. M. SHELXT− Integrated space-group and crystal-structure determination. *Acta Crystallogr., Sect. A: Found. Adv.* **2015**, *71*, 3−8.
(43) Macrae, C. F.; Edgington, P. R.; McCabe, P.; Pidcock, E.; Shields, G. P.; Taylor, R.; Towler, M.; van De Streek, J. Mercury: visualization and analysis of crystal structures. *J. Appl. Crystallogr.* **2006**, *39*, 453−457.
(44) Momma, K.; Izumi, F. VESTA 3 for three-dimensional visualization of crystal, volumetric and morphology data. *J. Appl. Crystallogr.* **2011**, *44*, 1272−1276.
(45) Song, L. X.; Robeyns, K.; Leyssens, T. Crystallizing Ionic Cocrystals: Structural Characteristics, Thermal Behavior, and Crystallization Development of a Piracetam-CaCl2 Cocrystallization Process. *Cryst. Growth Des.* **2018**, *18*, 3215−3221.
(46) Harmsen, B.; Leyssens, T. Enabling Enantiopurity: Combining Racemization and Dual-Drug Co-crystal Resolution. *Cryst. Growth Des.* **2018**, *18*, 3654−3660.
(47) Billot, P.; Hosek, P.; Perrin, M.-A. Efficient Purification of an Active Pharmaceutical Ingredient via Cocrystallization: From Thermodynamics to Scale-Up. *Org. Process Res. Dev.* **2013**, *17*, 505−511.

https://dx.doi.org/10.1021/acs.cgd.9b01725
Cryst. Growth Des. 2020, 20, 2602−2607